Available online at www.sciencedirect.com
SCIENCE DIRECT
Journal of the European Ceramic Society 26 (2006) 1947–1951
www.elsevier.com/locate/jeurceramsoc

Synthesis and characterisation of $La_{0.4}Ba_{0.6}Ti_{0.6}RE_{0.4}O_3$ (where RE = Y, Yb) ceramics

A. Feteira [a,*], R. Elsebrock [b], A. Dias [e], R.L. Moreira [c], M.T. Lanagan [d], D.C. Sinclair [a]

[a] *University of Sheffield, Department of Engineering Materials, Sir Robert Hadfield Building, Mappin Street, Sheffield S1 3JD, UK*
[b] *Research Centre Jülich, Institute of Solid State Research, 52425 Jülich, Germany*
[c] *Departamento de Física, ICEx, Universidade Federal de Minas Gerais, Caixa Postal 702, 30123-970, Belo Horizonte, Minas Gerais, Brazil*
[d] *Materials Research Institute, Penn State University, University Park, PA 16802, USA*
[e] *Departamento de Engenharia Metalúrgica e de Materiais, UFMG, Rua Espírito Santo 35, Belo Horizonte MG, 30160-030, Brazil*

Available online 17 November 2005

Abstract

$La_{0.4}Ba_{0.6}Ti_{0.6}RE_{0.4}O_3$ (where RE = Y, Yb) powders were synthesised by the mixed oxide route. According to laboratory X-ray diffractometry both compositions are single-phase and can be indexed on the $Pm\bar{3}m$ space group; however, electron diffraction suggests the occurrence of anti-phase octahedral tilting or 1:1 ordering. Ceramics fired at 1600 °C for 4 h exhibit an average grain size of ~20 μm. Bright field TEM images suggest the occurrence of chemical inhomogeneity in both compositions. The dc conductivities and Raman spectra are similar for both compositions; however, $La_{0.4}Ba_{0.6}Ti_{0.6}Y_{0.4}O_3$ ceramics exhibit $\varepsilon_r \sim 57$, quality factor (Qf) ~ 750 GHz and temperature coefficient of resonance (TCF) ~ 12 ppm/K, whereas $La_{0.4}Ba_{0.6}Ti_{0.6}Yb_{0.4}O_3$ ceramics exhibit $\varepsilon_r \sim 65$, $Qf \sim 4500$ GHz and TCF ~ 1 ppm/K.

Keywords: $BaTiO_3$ and titanates; Dielectric properties; Electron microscopy; Perovskites

1. Introduction

Recent progress in microwave telecommunication and satellite broadcasting has resulted in the need for materials with $\varepsilon_r \sim 60$–80, high quality factor ($Qf > 20{,}000$ GHz) and a near-zero temperature coefficient of resonant frequency (TCF).[1] Recently, the structure–property relations in the $x BaTiO_3$–$(1-x)La(Mg_{1/2}Ti_{1/2})O_3$ system have been investigated for these purposes.[1] For $x = 0.5$, $\varepsilon_r \sim 60$ and TCF ~ −2 ppm/K, however, Qf_r is only 9600 GHz, precluding any commercial application.

Considering that lanthanides have higher ion polarisability[2] than Mg^{2+} or Ti^{4+} (Table 1) we decided to investigate the microwave dielectric properties of rare-earth doped $BaTiO_3$ ceramics. Substitution of lanthanides in $BaTiO_3$ can occur either at the octahedral coordinated Ti-site or at the dodecahedrally coordinated Ba-site, depending mainly on the ionic radius of the lanthanide. The ionic radii of the lanthanide ions vary between that of Ba^{2+} and Ti^{4+}, as shown in Table 1.[3] It is generally accepted that ions from the start of the series (such as La^{3+}, Ce^{3+}) are incorporated exclusively at the Ba-site, whereas smaller ions (such as Yb^{3+}, Lu^{3+}) at the end of series primarily enter the Ti-site as demonstrated by Dunbar et al.[4] According to Zhi et al.,[5] the solubility of Y^{3+} on the Ba^{2+} site is ~1.5 at.% Y^{3+}, whereas on the Ti^{4+} site it is ~12.2 at.% Y^{3+}.

Recently, we have reported on the structure and low frequency dielectric properties of self-compensated $La_xBa_{1-x}Ti_{1-x}Y_xO_3$ ($0 \le x \le 0.45$) ceramics.[6] It was observed that the lattice constant a increases almost linearly with x, in agreement with Vegards law. This is a clear indication that Y^{3+} is incorporated on the B-site. The tolerance factors, $t = (r_A + r_O)/\sqrt{2}(r_B + r_O)$, (where r_A, r_B and r_O are the ionic radii of the A- and B-cations and oxygen ion, respectively) shown in Table 2 were then calculated considering that both Y and Yb are incorporated on the B-site. Hence, based on the relationship between tolerance factor and TCF, as observed by Reaney et al.,[7] solubility of $x > 0.35$ is sufficient to induce octahedral tilting and therefore tailor TCF near zero. In principle a self-compensated defect free lattice should exhibit low losses, providing that no other loss sources such as dc conductivity or clustering are predominant. Finally, the estimates of ε_r presented in Table 2 were calculated using the Clausius–Mosotti relation: $\varepsilon_r = (3V_m + 8\pi\alpha)/(3V_m - 4\pi\alpha)$,

* Corresponding author. Tel.: +44 114 226009; fax: +44 114 2225943.
E-mail address: a.feteira@sheffield.ac.uk (A. Feteira).

0955-2219/$ – see front matter © 2005 Elsevier Ltd. All rights reserved.
doi:10.1016/j.jeurceramsoc.2005.09.095

Table 1
Ionic radii and ion polarisability for some common lanthanide ions and Ba^{2+}, $Ti^{4+}$and Mg^{2+}

	Ba^{2+}	La^{3+}	Ce^{3+}	Nd^{3+}	Sm^{3+}	Gd^{3+}	Dy^{3+}	Y^{3+}	Yb^{3+}	Ti^{4+}	Mg^{2+}
VI (Å)	1.35	1.032	1.01	0.983	0.958	0.938	0.912	0.9	0.868	0.605	0.720
XII (Å)	1.61	1.36	1.34	1.27	1.24	–	–	–	–	–	–
α (Å^3)	6.40	6.07	6.15	5.01	4.74	4.37	4.07	3.81	3.58	2.93	1.32

Note: VI and XII correspond to ionic radii for 6- and 12-fold coordination (ref. 3), respectively, while α is the ion dielectric polarisability (ref. 2).

Table 2
Density, ε_r, quality factor, TCF and *t*-factor for $La_{0.4}Ba_{0.6}Ti_{0.6}RE_{0.4}O_3$ (RE = Yb, Y) ceramics

	ρ_{rel}	ε_r (calculated)	ε_r (experimental)	*Qf* (GHz)	TCF (ppm/K)	*t*-factor
LBTY	95.9	51	57	∼750	∼12	0.969
LBTYb	94.8	53	65	∼4500	∼1	0.975

where α and V_m are the ion polarisabilities and molecular volumes, respectively.

Here we present an investigation on the structure-property relationships of 'double-doped' $La_{0.4}Ba_{0.6}Ti_{0.6}RE_{0.4}O_3$ (where RE = Y, Yb) ceramics. The applicability of these two compositions as microwave dielectric resonators is then discussed.

2. Experimental

$La_{0.4}Ba_{0.6}Ti_{0.6}RE_{0.4}O_3$ (where RE = Y, Yb) ceramics were prepared by the mixed oxide route. The starting materials were high-purity grade $BaCO_3$, La_2O_3, Y_2O_3, Yb_2O_3 and TiO_2 powders. The required molar ratios were weighed and mixed by ball milling in propanol for 20 h. The dried slurries were calcined in air at 1400 °C. Purity and crystallinity were determined by X-ray diffraction using a high-resolution diffractometer (Cu $K\alpha_1$, 1.54059 Å) using a step size of 0.02° and a scan rate of 0.2°/min. The calcined powders were finely milled and shaped into pellets under an isostatic pressure of 200 MPa. The green compacts were fired at 1600 °C for 4 h in air, using a controlled heating and cooling rate of 5 and 3 °C/min, respectively. Microstructure of as-fired and thermally etched surfaces were examined using a scanning electron microscope (SEM) operated at 20 kV. Thin ceramic foils were examined by transmission electron microscopy (TEM). The room temperature dielectric properties at MW frequencies were measured by the resonant post method (Hakki and Courtney). Finally, micro-Raman scattering spectra were recorded using a Horiba/Jobin-Yvon spectrometer, equipped with a 1800 grooves/mm diffraction grating, a liquid-N_2-cooled CCD detector and a confocal microscope (10× objective). The experimental resolution was better than 1 cm^{-1}. After fitting, the ultimate resolution was 0.2 cm^{-1}. A helium-neon ion laser was used as the excitation source (power 12.5 mW).

3. Results and discussion

3.1. Crystal structure and microstructure

X-ray diffraction (XRD) revealed both compositions to be phase-pure (within the detection limits of the equipment) and the diffraction patterns could be indexed according to a simple cubic perovskite, space group $Pm\bar{3}m$, as illustrated in Fig. 1. The lattice constants were calculated as $a = 4.0930(4)$ and 4.1080(3) Å for LBTYb and LBTY, respectively. Electron diffraction patterns obtained along the ⟨1 0 0⟩, ⟨1 1 1⟩ and ⟨1 1 0⟩ zone axes are illustrated in Fig. 2a–c, respectively. Both ⟨1 0 0⟩ and ⟨1 1 1⟩ patterns can be indexed according to a cubic perovskite with lattice constant of ∼4 Å in agreement with the XRD data. Nevertheless, discrete superlattice reflections are visible at the $1/2\{h\,k\,l\}_p$ positions in the ⟨1 1 0⟩ zone axis pattern, as illustrated in Fig. 2c. These reflections can be associated either with 1:1 B-site atomic ordering or anti-phase octahedral tilting or even a combination of both.[7,8] Similar diffraction patterns were observed by Seabra et al.[1] in the $xBaTiO_3$–$(1-x)La(Mg_{1/2}Ti_{1/2})O_3$ system for compositions with $0.3 < x < 0.7$, where only anti-phase tilting was mentioned to be present. Structural refinement of the $La_{0.4}Ba_{0.6}Ti_{0.6}RE_{0.4}O_3$ (RE = Y, Yb) compositions is being carried out and the results will be reported in detail elsewhere.[9]

Microstructures for both ceramics consist of grains with an average size of ∼20 μm, as illustrated in Fig. 3 for LBTYb. The morphology of the grains is typical of liquid phase assisted sintering. Nanodomain contrast similar to that commonly observed in relaxors[10] was found in both compositions as illustrated by the bright field image in Fig. 4. This suggests the presence of randomly distributed clusters within the grains which is presumably associated with strain-effects induced by the difference in

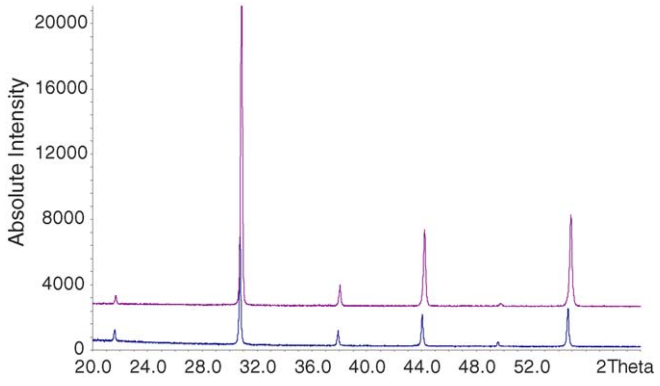

Fig. 1. X-ray diffraction patterns for LBTYb (top) and LBTY (bottom).

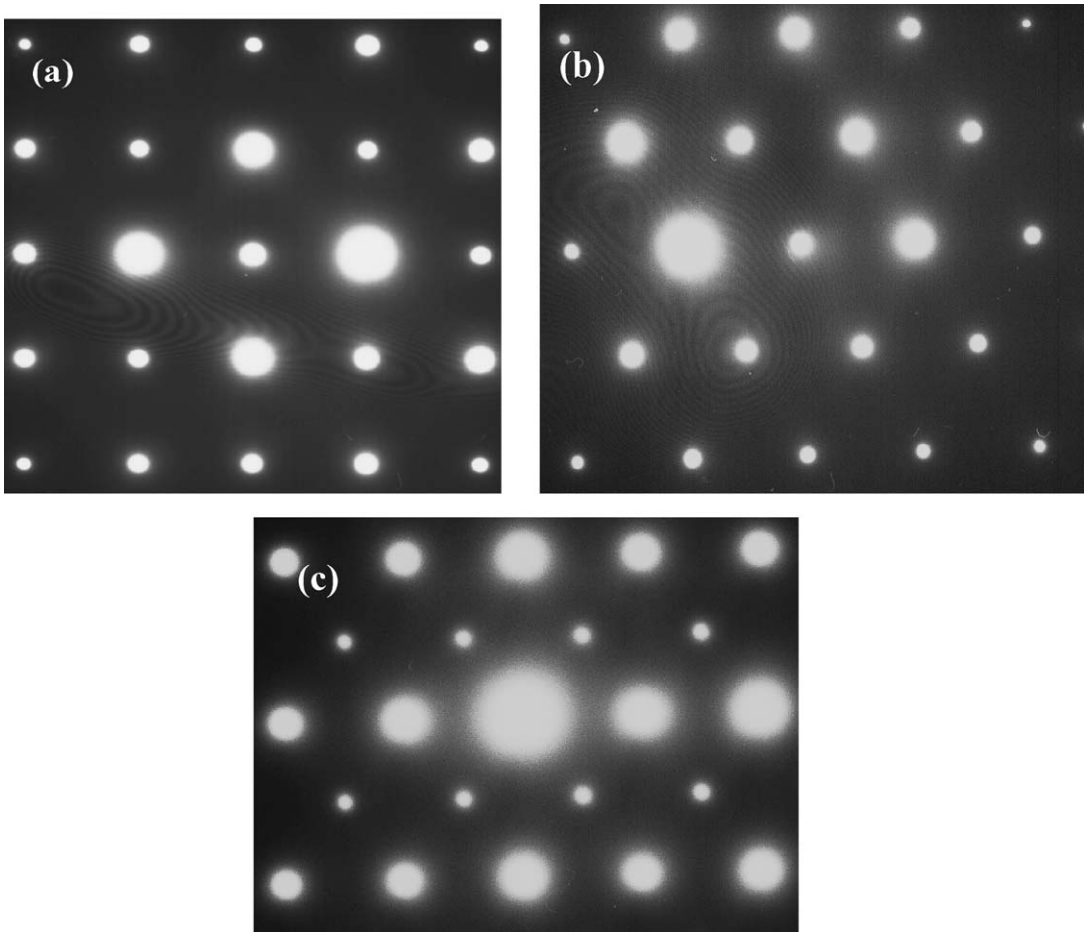

Fig. 2. Electron diffraction patterns along (a) ⟨1 0 0⟩, (b) ⟨1 1 1⟩ and (c) ⟨1 1 0⟩.

ionic radii of Ba^{2+} and La^{3+} on the A-site and Ti^{4+} and Yb^{3+} or Y^{3+} ions on the B-site of the unit cell. These considerable differences in ionic radii may induce localised regions of *uncorrelated* polarisation.

3.2. Microwave dielectric properties

Table 2 summarizes the microwave dielectric properties of $La_{0.4}Ba_{0.6}Ti_{0.6}RE_{0.4}O_3$ (RE = Y, Yb) ceramics. Data concerning relative density, estimated ε_r and tolerance factor are also included. LBTYb exhibits higher ε_r and the measured values are slightly larger than those predicted by the Clausius–Mosotti equation. The TCF value for LBTYb is close to zero, which is in good agreement with correlation between tolerance factor and TCF proposed by Reaney et al.[7] Surprisingly, LBTY exhibits a

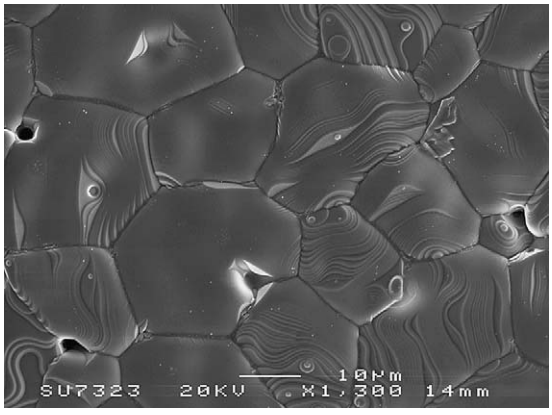

Fig. 3. SEM micrograph of LBTY 40 ceramics fired at 1600 °C for 4 h.

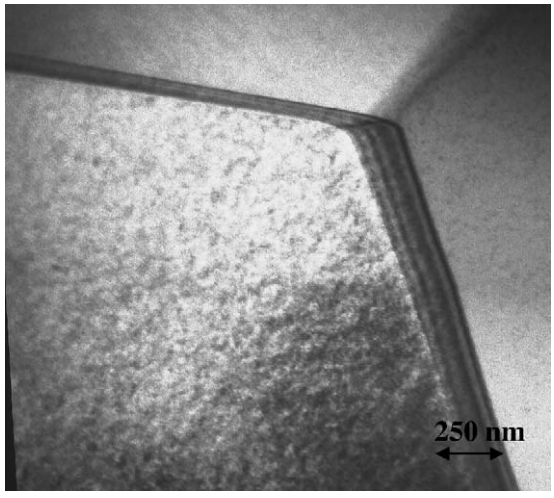

Fig. 4. TEM bright field image showing clustering in LBTYb 40 ceramics.

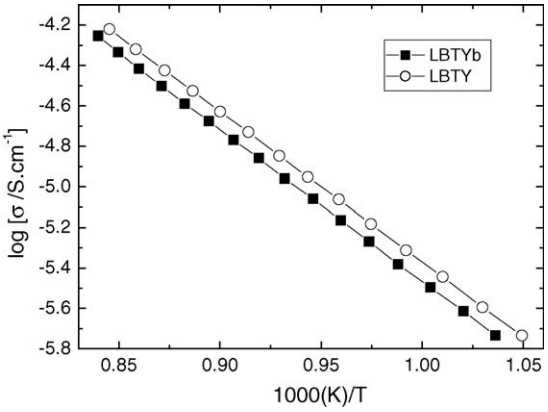

Fig. 5. Arrhenius plot of σ_{dc} for LBTYb and LBTY ceramics.

Qf value that is ~1 order of magnitude lower than that observed for LBTYb. The origin(s) of this difference is the subject of discussion in the following sections.

3.3. DC conductivity

Several authors[11,12] have found that even limited reduction of Ti^{4+} in titanate-based ceramics is sufficient to increase the dc conductivity and result in severe deterioration of *Qf*. dc bulk conductivity (σ_{dc}) data for $La_{0.4}Ba_{0.6}Ti_{0.6}RE_{0.4}O_3$ (Re = Y, Yb) ceramics are plotted against reciprocal temperature in Arrhenius format, Fig. 5. These data were extracted from complex impedance plots according to the methodology described elsewhere.[13] It is clear that LBTY and LBTYb have very similar conductivity values; however, they are ~3 orders of magnitude lower than those observed for undoped $BaTiO_3$ and $LaYbO_3$. Finally, the fact that the conductivity is similar for both compositions but that *Qf* differs by ~1 order of magnitude is a clear indication that the origin(s) of the losses in these materials are not associated with dc conductivity.

3.4. Raman spectroscopy

Raman spectra of LBTYb and LBTY in the frequency range 40–960 cm^{-1} are shown in Fig. 6. Eight strong bands are observed in both compositions, located at 99, 122, 155, 315, 416, 525, 713 and 780 cm^{-1}, for the LBTY sample. The ideal perovskite structure $Pm\bar{3}m$ does not show any Raman-active mode.[14] On the other hand, the presence of two different cations in A- or in B-positions leads to different possible superstructures, for which Raman scattering is allowed. From the eight observed bands, three are relatively unchanged with RE-ion substitution: the two lowest frequency modes (A-site motions) and the band at 415 cm^{-1} (BO_3 torsional bending mode). On the other hand, five bands presented some changes for the two compounds. Two bands located at 315 and 525 cm^{-1} (RE = Y) downshifted to 300 and 520 cm^{-1} with substitution by Yb, which is simply a mass effect. These bands are related to rotations of the oxygen cage and B–O stretching vibrations, respectively. On the other hand, three bands have the opposite behaviour, increasing the frequency from 155 cm^{-1} (A-site mode), 713 cm^{-1} (E oxygen mode) and 780 cm^{-1} (A_1 symmetric "breathing" of the BO_6 octahedra) for LBTY to 176, 720 and 785 cm^{-1}, for LBTYb. This result is probably an indication of an increase in the effective charge of oxygen for the Yb-based compound compared to the Y-based compound (since Y^{3+} has a larger ionic radius than Yb^{3+}, the RE–O bonds have higher covalency for the Y-based compound). Although the oxygen-related modes were sensitive to Y/Yb substitution, the differences in their behaviour are rather small to explain the higher difference in the *Qf* values.

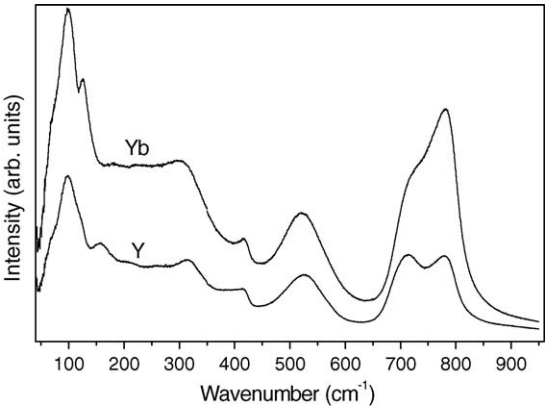

Fig. 6. Raman spectra for LBTYb (top) and LBTY (bottom).

A particular interesting case was described for $(A'_{1/2}A''_{1/2})(B'_{1/2}B''_{1/2})O_3$ perovskites, which showed cubic $F\bar{4}3m$ structure with eight Raman bands ($6F_2 + A_1 + E_1$).[14] The present results for LBTY and LBTYb are compatible with that trend, nevertheless, additional structural investigations are required to demonstrate, unequivocally, the space group(s) of these materials.

4. Conclusions

The results in this study confirm that the tolerance factor and the Clausius–Mosotti equation are both extremely useful relationships to use in the design of high ε_r ceramics with near-zero TCF; however, it is also demonstrated that the difference in ionic radii of ions on the same site is an important parameter that cannot be neglected. B-site clustering driven primarily by the difference of the ionic radii between Ti^{4+} and Y^{3+} and Yb^{3+} is suggested as the principal source for the microwave dielectric loss of $La_{0.4}Ba_{0.6}Ti_{0.6}RE_{0.4}O_3$ (Re = Y, Yb) ceramics, however, further structural studies are required to clarify the influence of crystal symmetry on *Qf*. Considering the large difference in ionic radii between Ba^{2+} and Ti^{4+} and most lanthanides, it should be expected that compositions based on $RE'_xBa_{1-x}Ti_{1-x}RE_xO_3$ formulations (where RE′ and RE are rare earths), are likely to be too lossy for commercial applications despite having high permittivity (>50) and near zero TCF for certain values of *x*.

Acknowledgments

We thank Dr. Ian Reaney (Sheffield University) for useful discussions and EPSRC for financial support. A. Dias and R.L.

Moreira acknowledge grants received from the Brazilian agencies CNPq and MCT.

References

1. Seabra, M. P., Avdeev, M., Ferreira, V. M., Pullar, R. C., Alford, N. M. and Reaney, I. M., Structure–property relations in $x\mathrm{BaTiO_3}$–$(1-x)\mathrm{La(Mg_{1/2}Ti_{1/2})O_3}$ solid solutions. *J. Am. Ceram. Soc.*, 2004, **87**(4), 584.
2. Shannon, R. D., Dielectric polarizabilities of ions in oxides and fluorides. *J. Appl. Phys.*, 1993, **73**(1), 348.
3. Shannon, R. D., Revised effective ionic radii and systematic studies of interatomic distances in halides and chalcogenides. *Acta Crystallogr. A*, 1976, **32**, 751.
4. Dunbar, T. D., Warren, W. L., Tuttle, B. A., Randall, C. A. and Tsur, Y., Electron paramagnetic resonance investigations of lanthanide-doped barium titanate: dopant site occupancy. *J. Phys. Chem. B*, 2004, **108**(3), 908.
5. Zhi, J., Chen, A., Zhi, Y., Vilarinho, P. M. and Baptista, J. L., Incorporation of yttrium in barium titanate ceramics. *J. Am. Ceram. Soc.*, 1999, **82**(5), 1345.
6. Feteira, A., Lanagan, M. T. and Sinclair, D. C., Microstructural and electrical characterisation of $\mathrm{La}_x\mathrm{Ba}_{1-x}\mathrm{Ti}_{1-x}\mathrm{Y}_x\mathrm{O}_3$ $(0 \le x \le 0.50)$ ceramics, *Key Eng. Mater.*, in press.
7. Reaney, I. M., Colla, E. L. and Setter, N., Dielectric and structural characteristics of Ba-based and Sr-based complex perovskites as a function of tolerance factor. *Jpn. J. Appl. Phys. Part 1—Regul. Pap. Short Notes Rev. Pap.*, 1994, **33**(7A), 3984.
8. Barber, D. J., Moulding, K. M., Zhou, J. and Li, M. Q., Structural order in $\mathrm{Ba(Zn_{1/3}Ta_{2/3})O_3}$, $\mathrm{Ba(Zn_{1/3}Nb_{2/3})O_3}$ and $\mathrm{Ba(Mg_{1/3}Ta_{2/3})O_3}$ microwave dielectric ceramics. *J. Mater. Sci.*, 1997, **32**(6), 1531.
9. Feteira, A., Gillie, L. and Sinclair, D. C., unpublished.
10. Zhang, R. T., Li, J. F. and Viehland, D., Effect of aliovalent substituents on the ferroelectric properties of modified barium titanate ceramics: relaxor ferroelectric behavior. *J. Am. Ceram. Soc.*, 2004, **87**(5), 864.
11. Templeton, A., Wang, X. R., Penn, S. J., Webb, S. J., Cohen, L. F. and Alford, N. M., Microwave dielectric loss of titanium oxide. *J. Am. Ceram. Soc.*, 2000, **83**(1), 95.
12. Kim, D. W., Ko, K. H., Kwon, D. K. and Hong, K. S., Origin of microwave dielectric loss in $\mathrm{ZnNb_2O_6}$–$\mathrm{TiO_2}$. *J. Am. Ceram. Soc.*, 2002, **85**(5), 1169.
13. Morrison, F. D., Sinclair, D. C. and West, A. R., Characterization of lanthanum-doped barium titanate ceramics using impedance spectroscopy. *J. Am. Ceram. Soc.*, 2001, **84**(3), 531.
14. Siny, I. G., Katiyar, R. S. and Bhalla, A. S., Cation arrangement in the complex perovskites and vibrational spectra. *J. Raman Spectrosc.*, 1998, **29**, 385.